Nuclear Inst. and Methods in Physics Research B 479 (2020) 47–50

Contents lists available at ScienceDirect

Nuclear Inst. and Methods in Physics Research B

journal homepage: www.elsevier.com/locate/nimb

Ion transmission through nanochannels: Energy dependent acceptance angle and transmission probability

Sjoerd Roorda*, Martin Chicoine

Département de physique, Université de Montréal, Canada

ARTICLE INFO

Keywords:
Ion beam analysis
Nanochannels
Channeling

ABSTRACT

The transmission of energetic (0.1–2 MeV) light ions through an array of parallel nanochannels was measured as a function of incident angle with respect to the channel axis. The angular transmission can be viewed macroscopically, similar to an ion passing through a collection of parallel slits which then determine the beam profile or similar to ion channeling in crystals. In the first case, the number of transmitted ions as a function of incident angle would be determined simply by the line-of-sight geometry (length over diameter) of the nanotube resulting in a critical angle of about 0.2° whereas in the second case, the acceptance angle would be much larger, nearly 0.8°, and analogous to the acceptance angle typically encountered in ion channeling in crystals. The measured critical angle varies between 0.4° and 0.8° depending on the incident ion energy, but with increasing energy the critical angle becomes larger rather than smaller. The transmittance at the optimal angle increases with energy and shows a strong linear correlation with it. This can be understood as a consequence of repeated interactions with the channel walls as the channeled ions travel along the channel.

1. Introduction

Anodic aluminum oxide (AAO) membranes consist of self-organized bundles of nanopores and have found a range of applications including biosensors [1], or can be used as a nanoscale template, for example as a mask for gold evaporation [2]. A particular template application is the use of such membranes as a mask for energetic ions, for example in reactive ion etching [3], ion beam processing [4], ion implantation for magnetic [5,6] or luminescent nanostructures [7]. The use of AAO membranes as ion implantation mask is not limited to thermal or low energy ions, they have been used for lithography of multi-MeV "swift heavy" ions [8] or as a mask to define a regular array of single swift heavy ion impact sites [9]. Other than AAO in the role of implantation mask, there has been work using ion beams to modify the membranes themselves [10]. Further development of all of these techniques would require an improved understanding of the ion transport properties of the nanochannels. Indeed, very little work on ion transport through nanochannels has been reported, other than a report on the nanochannel exit profile [11] and an observation of ion channeling in nanopores [12]. Here, we study ion transport throught AAO nanopores as an ion channeling phenomenon.

2. Critical angle for channeling

Ion channeling in crystals is well described by the Lindhard theory [13], which treats the "walls" of the channel formed by strings of atoms as a continuous potential. Lindhard derived a critical angle for channeling as $\Psi_1 = (2Z_1Z_2e^2/dE)^{1/2}$, where Z_1 and Z_2 are the incident particle and target atom atomic number, e the charge of the electron, d the interatomic distance along the channel wall (not the channel width) and E the energy of the incident ions. (When E is expressed in MeV and the angle is required in degrees, $\Psi_1 = 0.307(Z_1Z_2/dE)^{1/2}$ [14].) If nanochannels such as the 45 nm diameter nanopores through anodized aluminum oxide (AAO) behave in a similar fashion, one would expect a similarly large critical angle and a similar energy dependence of the critical angle. A much simpler view would be to regard ion transport through nanochannels as a small version of beam defining slits and assign a transmission probability of 1 if an ion can go straight through without hitting any obstacles and 0 otherwise. In that case, the aspect ratio of the nanochannel is the defining parameter for the angular distribution of the transmission probability, and in order to calculate the transmission probability as a function of incident angle, one evaluates the overlapping area of the two circles corresponding to the entrance and exit openings of the nanotube. The resulting curve has a distinctly non-gaussian shape with a sharp peak and, for a bundle of nanochannels with nanopore radius of $r = 22.5$ nm and a channel length of $L = 9\ \mu$m, a full width at half maximum of about 0.22°. We find that, in order to describe the transmission probability, neither description applies but that a combination of the two critical angles determines the ion transport efficiency.

* Corresponding author.
E-mail address: sjoerd.roorda@umontreal.ca (S. Roorda).

https://doi.org/10.1016/j.nimb.2020.05.026
Received 20 December 2019; Accepted 27 May 2020
Available online 18 June 2020
0168-583X/

3. Experiment

A self-supporting 9 µm thick anodic aluminum oxide membrane with highly aligned nanopores traversing the entire thickness of the membrane was prepared as described in an earlier paper [9]. The material surrounding the nanopores is amorphous unless annealed at a high temperature [15]. Image analysis of the front surface as seen in scanning electron microscopy (SEM) indicates that about 30% of the surface is "open". In our earlier work, 1.6 MeV Li ions were transmitted through the nanopores as a means of orienting the nanopores with the ion beam, and 70 MeV Ag ions were also transmitted. However, the transmission critical angle and efficiency were not studied in detail. Here, we used 100 keV to 2.7 MeV He ions and measured the transmitted current for a range of (horizontal and vertical tilt) angles ranging from -4° to 4° in steps of 0.1°. As the incident ion beam was quite stable over long periods of time and as the ion current measured on the membrane varied systematically when the tilt was varied, we simply measured the transmitted ion current with a Faraday cup positioned behind the membrane and normalized the charge thus collected by the average incident current times exposure time. At 2.7 MeV, some transmission was observed irrespective of tilt angle. The projected range R_p of 2.7 MeV He ions in Al_2O_3 is barely more than 6.2 µm [16]. We have not determined the density of the Al_2O_3 surrounding the nanopores, but if it is close to 3.69 g/cm^3 (the value used in the calculation of R_p), one can expect the actual R_p to be increased by the fraction of open volume (30%) in the membranes, or 8.9 µm. As a consequence, the membrane thickness of 9 µm is less than the expected penetration depth of R_p + 1 × straggle (0.23 µm) of 9.22 µm if the reduced density is taken into account. For 2 MeV and lower energy, no He ions were transmitted for tilt angles larger than a few degrees, but for some angles, ions were transmitted even when the energy was as low as 100 keV. The transmittance (transmitted charge/incident charge) of 2 MeV He ions as a function of horizontal and vertical tilt is shown in Fig. 1 as red circles (horizontal) and black squares (vertical). Red and black solid lines are Gaussian functions fit to the data; the dashed blue line close to 0 tilt is the expected transmission for a purely geometrical transmission mechanism, and the dotted red line indicates the critical angle for channeling according to Lindhard's expression, convoluted with the geometric transmission and the ion beam divergence.

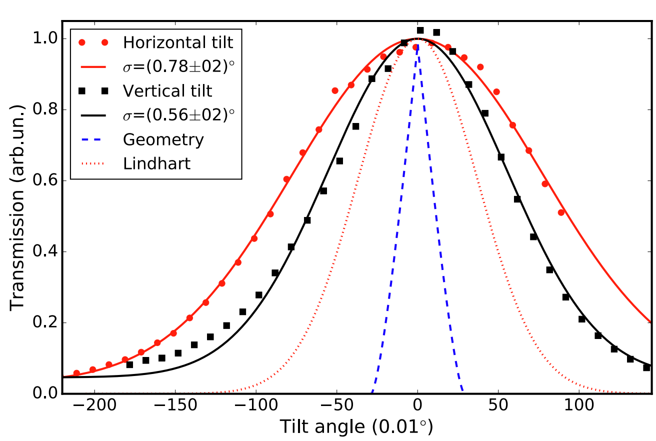

Fig. 1. He ions (2 MeV) transmitted through an AAO nanopore membrane. Red dots and black squares: measured transmitted ion current (normalized to maximum transmission) for horizontal and vertical angular scans, respectively. Red and black solid lines: gaussian fits to the experimental data with widths indicated in the figure legend. Dashed blue line: Calculated transmission based on a purely geometric, line-of-sight argument. Dotted red line: Convolution of geometric transmission with a gaussian distribution; the width corresponds to the quadratic sum of beam divergence (0.06°) and critical angle according to Lindhard [13]. (For interpretation of the references to colour in this figure legend, the reader is referred to the web version of this article.)

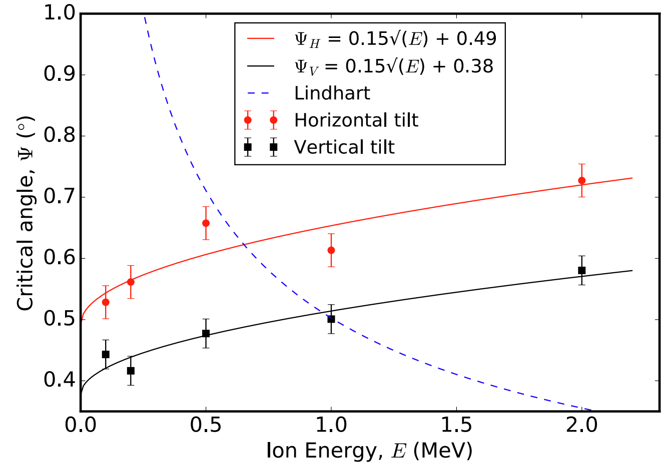

Fig. 2. Critical angle for He ions (0.1 – 2 MeV) transmitted through an AAO nanopore membrane. Red dots and black squares: Width of Gaussian fit to the transmittance as a function of a horizontal or vertical tilt of the sample normal relative to the incident ion beam direction, as a function of ion energy. Solid lines: Fit to the expression $a + b \times \sqrt{E}$, where the value for b was taken to be the same for vertical and horizontal tilt. Dashed blue line: Critical angle according to Lindhard theory [13]. (For interpretation of the references to colour in this figure legend, the reader is referred to the web version of this article.)

The experimental data is clearly much wider than profiles for the pure geometry or Lindhard theory. There is also a small difference in width for horizontal and vertical tilt. One possible and reasonable explantation for these discrepancies is the non-perfectness of the membrane: the nanopores are not perfectly parallel, and the membrane itself may be buckled. SEM images of similarly prepared membranes that were broken in two appear to show near perfect paralellism [9] but the field of view in the SEM is much smaller than the area probed by the ion beam which is about 1 mm diameter. Since any membrane-related effect would be independent of incident ion energy, we reduced the ion energy and measured again. The results are shown in Fig. 2 which shows the width of vertical and horizontal scans, as deduced by fitting a 2D gaussian to the ion transmission data, as a function of incident ion energy. As the energy is reduced, the transmission curve becomes narrower, instead of larger as expected from Lindhard theory or unchanged if the nanopore geometry were the sole deciding factor. We decided to fit the data to an expression which is the sum of a fixed, energy-independent width due to membrane non-parallelism, and an energy dependent part which we presumed to depend on the square root of ion energy, $\Psi(E) = \Psi_{np} + \Psi_E = \Psi_{np} + C\sqrt{E}$, where Ψ_{np} is the width due to non-paralellism of the nanopores, Ψ_E the energy dependent term and C a constant. We presumed that Ψ_{np} can be different for vertical and horizontal tilt, but that Ψ_E is the same in both scans. The fits are shown in the figure as solid lines. The blue dashed line depicts the energy dependence according to Lindhard theory.

These fits show that there is indeed a significant energy-independent contribution to the width of the transmission curve, $(0.50 \pm 0.03)^\circ$ for the horizontal and $(0.36 \pm 0.03)^\circ$ for the vertical scan, and the energy dependent part can be written as $(0.15 \pm 0.03)^\circ \times \sqrt{E}$, where E in MeV. The choice of a $\sqrt{E}$ dependence was inspired by the $1/\sqrt{E}$ dependence of the Lindhard critical angle, but inspection of Fig. 2 shows that a fit with a linear energy dependence would result in equally good agreement. In either case, the difference between our data and Lindhard theory is striking, and we suggest that such is the case because we measure *transmission* rather than *channeling*: the transmitted ions reaching the Faraday cup only include those that were not only channeled into the nanopore, but did not experience any de-channeling along the way. In Fig. 3 we show the maximum transmittance, that is the optimal value of (transmitted charge/incident charge) as a function of ion energy. In the figure, points correspond to data points and the

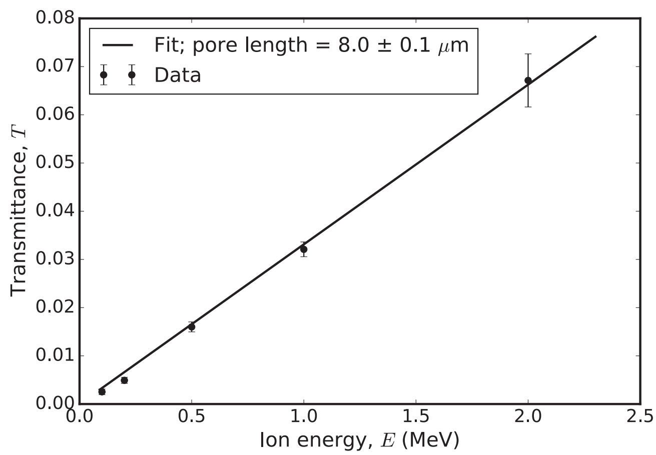

Fig. 3. Maximum transmission of He ions through an aligned AAO nanopore membrane as a function of incident energy. Black dots: data. Line: linear fit.

solid line is a linear fit. Note that even at 2 MeV the maximum transmittance is less than 8%, whereas the fraction of open volume, as deduced from SEM, is 30%, indicating that some dechanneling must have taken place. Also shown in the figure, as a solid line, is the transmittance according to a very simple model to be discussed next.

4. Critical angle for transmission

There is a clear correlation between the energy dependence of the transmittance and the critical solid angle for transmission. Indeed, for low incident ion energy, the critical angle for transmission is much reduced from the Lindhard value, and the transmittance is much reduced as well. In order to understand this behaviour, consider two ions with different energy but both at the critical angle according to Lindhard. Their lateral momenta are identical, but their momenta along the channel direction are very different. The interaction with the channel walls is intermittent: an ion encounters the potential wall of the channel, its lateral velocity is reduced, and reversed. It then travels relatively unencombered through the vacuum of the channel center, until it encounters the other wall. For a slow ion, the two interaction points are at a relatively short interval along the channel depth, whereas for the fast ion, a larger distance separates the two interaction zones. Since each interaction region carries with it the possibility of a close encounter with a nucleus and therefore a de-channeling event, the low energy ion has a much larger probability to de-channel, and only slow ions with a suitably low lateral momentum (i.e., an incident angle smaller than the Lindhard critial angle) will be transmitted by the nanopore. We now consider a very simple expression for the transmission probability: let us require that after the first wall interaction (or channeling event) a channelled ion is only transmitted if it manages to exit the nanopore without hitting the other wall (which, after all, is not likely to be as atomically flat as a channel in a perfect crystal). This restricts the transmission to channeled ions within a cone defined by the nanopore geometry, a fraction equal to $(\Psi_{geo}/\Psi_1)^2$, where $\Psi_{geo} = \arctan(2r/l)$ for a nanopore with radius r and length l and Ψ_1 the (energy dependent) Lindhard critical angle. This expression, linear in ion energy dependence, was fit to the data shown in Fig. 3 with one free parameter (the nanopore length l) which was found to be 8.0 ± 0.1 μm. Given the membrane thickness of 9 μm, this simple model works surprisingly well and seems to indicate that a second wall interaction event is enough to de-channel most channeled ions.

The depth distribution of ions implanted into an amorphous solid can be described by a Pearson IV distribution with suitable parameters [17] or calculated by SRIM, a code based on a large collection of ion implantation data [16]. For ions implanted along a major crystal axis of a monocrystalline target, the situation is more complicated, but such channeled ions do penetrate more deeply than non-channeled ions, and the larger the crystal channel, the deeper the channeled ions penetrate [18]. For our samples, 2.7 MeV He ions are transmitted irrespective of tilt angle even though the projected range plus straggle of 6.5 μm (according to SRIM [16] in dense Al_2O_3) is less than the membrane thickness (9 μm), because the nanopore membrane has a 30% density deficit. For 100 keV He ions, the projected range plus straggle is less than 0.5 μm, and therefore the range extension through channeling is more than a factor of 12 albeit at the price of a much reduced transmission.

At the outset, the possible application of AAO nanopore membranes as a mask for ion implantation was mentioned. Our results on the critical angle for transmission have implications for such use: Since the transmitted ions travel within a narrow cone defined by the nanopore geometry (Ψ_{geo}) one may expect that succesfull patterning can be obtained at relatively large distance from the nanopore exit.

5. Conclusion

In conclusion, we have measured the transmission of 0.1–2 MeV He ions through a self-supported anodic aluminum oxide membrane with aligned, 45 nm diameter nanopores traversing the entire 9 μm membrane thickness. Even though the ion energy required to penetrate such a thickness of Al_2O_3 exceeds 2 MeV, we have seen transmission of 100 keV ions. The critical angle for transmission decreases for lower energies, a type of behaviour opposite to the energy dependence of ion channeling in crystals. However, this behaviour can be understood as a consequence of interaction between the channel walls and the channeled ions, where low energy ions suffer more dechanneling than high energy ones, so that the fraction of transmitted ion scales linearly with ion energy.

Declaration of Competing Interest

The authors declare that they have no known competing financial interests or personal relationships that could have appeared to influence the work reported in this paper.

Acknowledgements

This work was financially supported by the Natural Sciences and Engineering Research Council of Canada (NSERC) and the Fonds de Recherche Québec, Nature et Technologies (FQRNT).

References

[1] A.M.M. Jani, D. Losic, N.H. Voelcker, Nanoporous anodic aluminium oxide: advances in surface engineering and emerging applications, Prog. Mater Sci. 58 (5) (2013) 636–704.
[2] H. Masuda, M. Satoh, Fabrication of gold nanodot array using anodic porous alumina as an evaporation mask, Jpn. J. Appl. Phys. 35 (1B) (1996) L126.
[3] S.G. Cloutier, C.-H. Hsu, P.A. Kossyrev, J. Xu, Enhancement of radiative recombination in silicon via phonon localization and selection-rule breaking, Adv. Mater. 18 (7) (2006) 841–844.
[4] E. Menéndez, A. Martinavicius, M. Liedke, G. Abrasonis, J. Fassbender, J. Sommerlatte, K. Nielsch, S. Suriñach, M. Baró, J. Nogués, et al., Patterning of magnetic structures on austenitic stainless steel by local ion beam nitriding, Acta Mater. 56 (17) (2008) 4570–4576.
[5] S. Shin, S. Lee, J. Lee, C. Whang, J. Lee, I. Choi, T. Kim, J. Song, Ion-beam nanopatterning by using porous anodic alumina as a mask, Nanotechnology 16 (8) (2005) 1392.
[6] J. Jensen, R. Sanz, M. Jaafar, M. Hernández-Vélez, A. Asenjo, A. Hallén, M. Vázquez, Localized $^{56}Fe^{+}$ ion implantation of TiO_2 using anodic porous alumina, MRS Online Proceedings Library Archive (2009) 1181.
[7] E. Rotem, J.M. Shainline, J.M. Xu, Electroluminescence of nanopatterned silicon with carbon implantation and solid phase epitaxial regrowth, Opt. Express 15 (21) (2007) 14099–14106.
[8] R. Sanz, J. Jensen, A. Johansson, M. Skupinski, G. Possnert, M. Boman, M. Hernandez-Velez, M. Vazquez, K. Hjort, Well-ordered nanopore arrays in rutile TiO_2 single crystals by swift heavy ion-beam lithography, Nanotechnology 18 (30) (2007) 305303.

[9] X. Cauchy, S. Roorda, Nearly equidistant single swift heavy ion impact sites through nanoporous alumina masks, in: AIP Conference Proceedings, vol. 1525, AIP, 2013, pp. 375–379.
[10] Y.-S. Bae, J. Jeon, C.-H. Jung, D. Choi, Experimental study on physical properties of nanoporous anodic aluminum oxide by proton implantation, J. Mech. Sci. Technol. 28 (8) (2014) 3219–3222.
[11] W. Guan, I.M. Ross, U.M. Bhatta, J. Ghatak, N. Peng, B.J. Inkson, G. Möbus, Nanopatterning by ion implantation through nanoporous alumina masks, Phys. Chem. Chem. Phys. 15 (12) (2013) 4291–4296.
[12] E. Muratova, A. Shemukhin, Nanoscale matrices to transport high-energy beams, in: Journal of Physics: Conference Series, vol. 917, IOP Publishing, 2017, p. 092016.
[13] J. Lindhard, Influence of crystal lattice on motion of energetic charged particles, Mat. Fys. Medd. Dan. Vid. Selsk. 34 (13) (1965).
[14] W.-K. Chu, J.W. Mayer, M.-A. Nicolet, Backscattering Spectroscopy, Academic Press, New York, 1978.
[15] S. Yang, T. Li, L. Huang, T. Tang, J. Zhang, B. Gu, Y. Du, S. Shi, Y. Lu, Stability of anodic aluminum oxide membranes with nanopores, Phys. Lett. A 318 (4–5) (2003) 440–444.
[16] J.F. Ziegler, M.D. Ziegler, J.P. Biersack, SRIM–the stopping and range of ions in matter (2010), Nucl. Instrum. Methods Phys. Res. Sect. B 268 (11–12) (2010) 1818–1823.
[17] R.G. Wilson, The Pearson IV distribution and its application to ion implanted depth profiles, Rad. Effects 46 (3–4) (1980) 141–147.
[18] G. Dearnaley, J. Freeman, G. Gard, M. Wilkins, Implantation profiles of 32P channeled into silicon crystals, Can. J. Phys. 46 (6) (1968) 587–595.